SLAC – PUB – 4346
June 1987
(T/E)

Resonant Substructure in $K\pi\pi$ Decays of Charmed D Mesons*

J. Adler, J.J. Becker, G.T. Blaylock, T. Bolton, J.S. Brown, K.O. Bunnell, T.H. Burnett, R.E. Cassell, D. Coffman, V. Cook, D.H. Coward, D.E. Dorfan, G.P. Dubois, A.L. Duncan, G. Eigen, K.F. Einsweiler, B.I. Eisenstein, T. Freese, G. Gladding, C. Grab, F. Grancagnolo, R.P. Hamilton, J. Hauser, C.A. Heusch, D.G. Hitlin, J. M. Izen, L. Köpke, A. Li, W.S. Lockman, U. Mallik, C.G. Matthews, R. Mir, P.M. Mockett, R.F. Mozley, B. Nemati, A. Odian, L. Parrish, R. Partridge, J. Perrier, D. Pitman, S.A. Plaetzer, J.D. Richman, H.F.W. Sadrozinski, M. Scarlatella, T.L. Schalk, R.H. Schindler, A. Seiden, C. Simopoulos, A.L. Spadafora, I.E. Stockdale, W. Stockhausen, J.J. Thaler, W. Toki, B. Tripsas, F. Villa, S. Wasserbaech, A. Wattenberg, A.J. Weinstein, N. Wermes, H.J. Willutzki, D. Wisinski, W.J. Wisniewski, R. Xu, Y. Zhu

The MARK III Collaboration

California Institute of Technology, Pasadena, CA 91125
University of California at Santa Cruz, Santa Cruz, CA 95064
University of Illinois at Urbana-Champaign, Urbana, IL 61801
Stanford Linear Accelerator Center, Stanford, CA 94305
University of Washington, Seattle, WA 98195

ABSTRACT

Dalitz plot analyses of four $K\pi\pi$ decays of the D^0 and D^+ mesons are presented. The relative amounts of $\bar{K}^*\pi$, $\bar{K}\rho$ and non–resonant $K\pi\pi$ in each decay mode are determined, and isospin amplitudes and phases are derived. These results are compared with predictions from QCD. The $K^-\pi^+\pi^+$ mode has a non–uniform, non–resonant contribution; attempts to fit this distribution are described.

Submitted to *Physics Letters*

* Work supported in part by the Department of Energy, under contracts DE-AC03-76SF00515, DE-AC02-76ER01195, DE-AC03-81ER40050, DE-AM03-76SF00034, and by the National Science Foundation.

The study of pseudoscalar–pseudoscalar (PP) and pseudoscalar–vector (PV) hadronic decays of the D mesons provides information on the mechanisms of heavy quark decay and subsequent hadronization.[1,2,3] The ratios $B(D^0 \to \bar{K}^{*0}\pi^0)/B(D^0 \to K^{*-}\pi^+)$ and $B(D^0 \to \bar{K}^0\rho^0)/B(D^0 \to K^-\rho^+)$ can distinguish between models which require the W–exchange diagram[4] and those that modify perturbative QCD calculations.[5] The presence of final state interactions[5] can be established. Predictions for the branching fractions of non–resonant decays to three pseudoscalar mesons[6] can be tested once the resonant decays are subtracted. Previous measurements[7] have been dominated by statistical errors. The Mark III data sample has sufficient statistics in the Cabibbo allowed three–body decays of the D mesons to provide accurate measurements of these branching fractions.

Presented herein are Dalitz plot analyses of four decays of the charmed D^0 and D^+ mesons:[8] $D^0 \to K^-\pi^+\pi^0$, $D^0 \to \bar{K}^0\pi^+\pi^-$, $D^+ \to \bar{K}^0\pi^+\pi^0$, and $D^+ \to K^-\pi^+\pi^+$. The data sample consists of an integrated luminosity of 9.3 pb^{-1} collected on the peak of the $\psi(3770)$ resonance with the Mark III detector[9] at SPEAR.

Candidate $D \to K\pi\pi$ decays are selected with the procedure used in an earlier analysis of D meson branching fractions.[10] Pairs of D mesons are produced in the decay of the $\psi(3770)$, with each D carrying the beam energy. This "beam constraint" is imposed when calculating the invariant mass of the $K\pi\pi$ system. In decay modes involving π^0's, constraints on the $\gamma\gamma$ invariant mass and the $K\pi\pi^0$ energy are simultaneously applied.[11] These constraints significantly improve the mass resolution of the $K\pi\pi$ system and provide rejection of background from incorrect particle associations and non–charm hadron production. Events with a beam–constrained mass within 5 MeV/c^2 (3 MeV/c^2 in the case of $K^-\pi^+\pi^+$) of the nominal D mass are selected for further study. The resolution of the invariant mass squared of the particle pairs used in the Dalitz plots is ~ 0.015 (GeV/c^2)^2.

The fractions of PV and non–resonant three–body contributions to each de-

cay mode are determined by fitting the Dalitz plot distributions to a coherent sum of amplitudes using a maximum–likelihood method. The three–body amplitude A_{3b} is assumed to be constant over the Dalitz plot. Relativistic Breit–Wigner amplitudes (BW), which include the vector decay matrix elements and mass–dependent widths,[12] are used to parameterize the K^* and ρ decays. The likelihood functions ($\mathcal{L}_{sig}$) are expressed as double differentials in the Dalitz plot variables $m^2_{\pi_1\pi_2}, m^2_{K\pi_1}$. They take the following forms for the $K^-\pi^+\pi^0$, $\bar{K}^0\pi^+\pi^-$, $\bar{K}^0\pi^+\pi^0$, and $K^-\pi^+\pi^+$ Dalitz plots, respectively:

$$\mathcal{L}^{-+0}_{sig} = |f_1 e^{i\phi_1} A_{3b} + f_2 e^{i\phi_2} BW_{\rho^+} + f_3 e^{i\phi_3} BW_{K^{*-}} + f_4 e^{i\phi_4} BW_{\bar{K}^{*0}}|^2 \qquad (1)$$

$$\begin{aligned}\mathcal{L}^{0+-}_{sig} =& |f_5 e^{i\phi_5} A_{3b} + f_6 e^{i\phi_6} BW_{\rho^0} + f_7 e^{i\phi_7} BW_{K^{*-}}|^2 \\ &+ |f_5 e^{i\phi_5} A_{3b} + f_6 e^{i\phi_6} BW_{\rho^0} + f_7 e^{i\phi_7} BW_{K^{*+}}|^2\end{aligned} \qquad (2)$$

$$\mathcal{L}^{0+0}_{sig} = |f_8 e^{i\phi_8} A_{3b} + f_9 e^{i\phi_9} BW_{\rho^+} + f_{10} e^{i\phi_{10}} BW_{K^{*0}}|^2 \qquad (3)$$

$$\mathcal{L}^{-++}_{sig} = |f_{11} e^{i\phi_{11}} A_{3b} + f_{12} e^{i\phi_{12}} B_{3b} + f_{13} e^{i\phi_{13}} BW_{\bar{K}^{*0}_1} + f_{13} e^{i\phi_{13}} BW_{\bar{K}^{*0}_2}|^2 \qquad (4)$$

where f_i are the coefficients for each contribution to the Dalitz plot and the ϕ_i are the relative phases.[13] The $K^-\pi^+\pi^+$ Dalitz plot contains a non–uniform, non–resonant contribution parameterized by a function B_{3b} to be discussed below. The likelihood functions, including detection efficiency, are normalized across the Dalitz plot using Monte Carlo $K\pi\pi$ events generated according to three–body phase space, and subjected to the same analysis as the data.

The distribution of background events under the D signal in each mode is parameterized by adding a term to the likelihood function which describes the variation of the background across the Dalitz plots. The background term is determined by fitting a sample of background events with beam–constrained mass between 1.82 and 1.85 GeV/c^2 to a two dimensional cubic polynomial.[14] The background samples show no evidence of resonant substructure in any of the

decay modes. A fit to the beam–constrained mass distribution determines the ratio of background to signal in the event sample used in the Dalitz plot analyses.

The fit results are presented in Table 1[15] and illustrated in Figs. 1–4. Our definition of the branching fraction[16] implies that the fractions of events from each component will not always sum to one because the interference terms do not necessarily integrate to zero. In each mode the best fit requires coherence between all resonant and non–resonant amplitudes, except in the $\bar{K}^0\pi^+\pi^-$ mode, where the best fit slightly favors incoherence between the resonant contributions and the non–resonant three-body amplitude.

The $K^-\pi^+\pi^+$ Dalitz plot has unique features.[7] Since this final state contains identical charged pions, the Dalitz plot must be folded (Fig. 4). A large non–resonant contribution interferes with the $\bar{K}^{*0}\pi^+$ amplitude, shifting the K^* peak to low masses at one end of the band and to high masses at the other end, where the K^* decay matrix element changes sign. The non–resonant contribution is not distributed according to phase space, but accumulates in the region where $m^2_{K\pi_1}$ approaches $m^2_{K\pi_2}$. To accommodate this distribution it is necessary to add an *ad hoc* term to the likelihood function. The best fit is obtained with a Bose symmetric term of the form $B_{3b} = |m^2_{K\pi_1} - m^2_{K\pi_2}|$. No evidence is found for any known[17] or hypothesized $K\pi$ resonances (other than the $K^*(892)$), exotic $\pi^+\pi^+$ states, or non–resonant P–wave $K\pi$ or D–wave $\pi\pi$ amplitudes. Since B_{3b} changes rapidly in the K^{*0} region, much of the apparent K^{*0} signal is attributed by the fit to interference.

To evaluate the goodness of fit, the data are binned in a two dimensional histogram and three projections. The fit results, normalized to the number of data events, are then compared to the binned data, and a χ^2 is evaluated for each histogram.[18] The χ^2 per degree of freedom is close to one for all of the two dimensional histograms and projections shown in the figures. No systematic deviation between the binned data and fit results is observed in any region of the Dalitz plots.

Table 1 $D \to K\pi\pi$ Fit Results

Decay Mode	Fit Fraction (%)	Phase (degrees)	$\sigma \cdot B$[15] (nb)	Branching Fr.[15] (%)
$K^-\pi^+\pi^0$			$0.76 \pm 0.04 \pm 0.08$	$13.3 \pm 1.2 \pm 1.3$
$K^-\rho^+$	$81 \pm 3 \pm 6$	0.0	$0.62 \pm 0.02 \pm 0.09$	$10.8 \pm 0.4 \pm 1.7$
$K^{*-}\pi^+$	$12 \pm 2 \pm 3$	154 ± 11	$0.28 \pm 0.04 \pm 0.08$	$4.9 \pm 0.7 \pm 1.5$
$\bar{K}^{*0}\pi^0$	$13 \pm 2 \pm 3$	7 ± 7	$0.15 \pm 0.02 \pm 0.04$	$2.6 \pm 0.3 \pm 0.7$
non–res.	$9 \pm 2 \pm 4$	52 ± 9	$0.07 \pm 0.02 \pm 0.03$	$1.2 \pm 0.2 \pm 0.6$
$\bar{K}^0\pi^+\pi^-$			$0.37 \pm 0.03 \pm 0.03$	$6.4 \pm 0.5 \pm 1.0$
$\bar{K}^0\rho^0$	$12 \pm 1 \pm 7$	93 ± 30	$0.04 \pm 0.01 \pm 0.02$	$0.8 \pm 0.1 \pm 0.5$
$K^{*-}\pi^+$	$56 \pm 4 \pm 5$	0.0	$0.31 \pm 0.02 \pm 0.05$	$5.3 \pm 0.4 \pm 1.0$
non–res.	$33 \pm 5 \pm 10$	–	$0.12 \pm 0.02 \pm 0.04$	$2.1 \pm 0.3 \pm 0.7$
$\bar{K}^0\pi^+\pi^0$			$0.42 \pm 0.08 \pm 0.08$	$10.2 \pm 2.5 \pm 1.6$
$\bar{K}^0\rho^+$	$68 \pm 8 \pm 12$	0.0	$0.29 \pm 0.03 \pm 0.09$	$6.9 \pm 0.8 \pm 2.3$
$\bar{K}^{*0}\pi^+$	$19 \pm 6 \pm 6$	43 ± 23	$0.24 \pm 0.07 \pm 0.10$	$5.9 \pm 1.9 \pm 2.5$
non–res.	$13 \pm 7 \pm 8$	250 ± 19	$0.05 \pm 0.03 \pm 0.04$	$1.3 \pm 0.7 \pm 0.9$
$K^-\pi^+\pi^+$			$0.39 \pm 0.01 \pm 0.03$	$9.1 \pm 1.3 \pm 0.4$
$\bar{K}^{*0}\pi^+$	$13 \pm 1 \pm 7$	105 ± 8	$0.08 \pm 0.01 \pm 0.04$	$1.8 \pm 0.2 \pm 1.0$
non–res.	$79 \pm 7 \pm 15$	0.0	$0.31 \pm 0.03 \pm 0.10$	$7.2 \pm 0.6 \pm 1.8$

The systematic errors on the fit fractions are estimated by varying the event selection criteria, the method of background determination, the method of efficiency determination, and the pattern of interference between contributions. The largest sources of systematic error are the π^0 reconstruction efficiency and the parameterization of the background. In the $K^-\pi^+\pi^+$ mode, no systematic error has been included for the parameterization of the non–uniform, non–resonant contribution.

Comparisons of PV branching fractions measured in two distinct final states

show good agreement for $B(D^0 \to K^{*-}\pi^+)$ but poor agreement for $B(D^+ \to \bar{K}^{*0}\pi^+)$ (see Table 1). The discrepancy in the latter mode suggests that while the likelihood function $\mathcal{L}_{sig}^{-++}$ provides a good fit to the data, the form of B_{3b} chosen does not adequately describe the physics. In the comparisons that follow, the results from the fit to the $K^-\pi^+\pi^+$ mode will not be used.

Recent extensions of the spectator model of D meson decay adequately account for the pattern of PP decays either by the addition of new amplitudes (*e.g.*, W–exchange[4]) or by the modification of the effective coefficients of the hadronic matrix elements.[5] To distinguish between these two corrections to the naive spectator picture, their predictions for PV decays may be evaluated against the measurements presented here. Table 2 compares two representative models, those of Kamal[4] (Model 1) and of Stech and collaborators[5] (Model 2).

Table 2 Decay Width Ratios Compared with Theory

Ratio	This Expt	Model 1[4]	Model 2[5]
$\frac{\Gamma(D^0\to\bar{K}^{*0}\pi^0)}{\Gamma(D^0\to K^{*-}\pi^+)}$	$0.50 \pm 0.07 \pm 0.15$	0.124 – 0.271	0.43
$\frac{\Gamma(D^0\to\bar{K}^{0}\rho^0)}{\Gamma(D^0\to K^{-}\rho^+)}$	$0.07 \pm 0.01 \pm 0.04$	0.036 – 0.135	0.08

Model 2 is favored, suggesting that deviations from the spectator picture arise from non–perturbative contributions to the QCD coefficients.

The importance of final state interactions is emphasized in both models. This is observed in the data as phase shifts between isospin amplitudes. The isospin amplitudes $A_{\frac{1}{2}}$, $A_{\frac{3}{2}}$ and phase shifts $\delta_{\frac{1}{2}}$, $\delta_{\frac{3}{2}}$ have been defined, for example, in reference 2. From Table 1, the ratio of isospin amplitudes is determined to be:

$$D \to \bar{K}\rho: \quad |A_{\frac{1}{2}}/A_{\frac{3}{2}}| = 3.12 \pm 0.40, \quad \delta_{\frac{1}{2}} - \delta_{\frac{3}{2}} = (0 \pm 26)^\circ$$

$$D \to \bar{K}^*\pi: \quad |A_{\frac{1}{2}}/A_{\frac{3}{2}}| = 3.22 \pm 0.97, \quad \delta_{\frac{1}{2}} - \delta_{\frac{3}{2}} = (84 \pm 13)^\circ$$

$$D \to \bar{K}\pi: \quad |A_{\frac{1}{2}}/A_{\frac{3}{2}}| = 3.67 \pm 0.27, \quad \delta_{\frac{1}{2}} - \delta_{\frac{3}{2}} = (77 \pm 11)^\circ$$

where the last set is derived from reference 11. The existence of isospin amplitude

phase shifts indicates sizeable final state interactions in the $\bar{K}\pi$ and $\bar{K}^*\pi$ modes.

We gratefully acknowledge the efforts of the SPEAR staff. We also wish to thank I.I.Y. Bigi, H. Haber, T. Banks, and M. Peskin for useful discussions. This work was supported in part by the U.S. National Science Foundation and the U.S. Department of Energy under contracts No. DE-AC03-76SF00515, No. DE-AC02-76ER01195, No. DE-AC03-81ER40050, and No. DE-AM03-76SF00034.

REFERENCES

1. For a recent review, see R. Schindler, SLAC–PUB–4135 (1986), to be published in **High Energy Electron–Positron Physics** (World Scientific Publishing Co.)

2. R. Rückl, Habilitationschrift Univ. Munchen (1983).

3. L. L. Chau, Phys.Rep. **95** (1983) 1; L. L. Chau and H. Y. Cheng, Phys. Rev. Lett. **56** (1986) 1655.

4. A. N. Kamal, SLAC–PUB–3443 (1984) (unpublished); A. N. Kamal, Phys. Rev. **D33** (1986) 1344.

5. D. Fakirov and B. Stech, Nucl. Phys. **B133**, (1978) 315; M. Bauer and B. Stech, Phys. Lett. **152B** (1985) 380; M. Bauer, B. Stech and M. Wirbel, Z. Phys **C34** (1987) 103.

6. H. Y. Cheng, Z. Phys. **C32** (1986) 243.

7. J. E. Wiss *et al.*, Phys. Rev. Lett. **37** (1976) 1531; R. H. Schindler *et al.*, Phys. Rev. **D24** (1981) 78.

8. Throughout this paper we adopt the convention that reference to a state also implies reference to its charged conjugate.

9. D. Bernstein *et al.*, Nucl. Inst. Meth. **226** (1984) 301.

10. R. M. Baltrusaitis *et al.*, Phys. Rev. Lett. **56** (1986) 2140.

11. J. Hauser, Ph.D. thesis, California Institute of Technology, CALT-68-1275 (1985).

12. J. D. Jackson, Nuovo Cimento **34** (1964) 1644; J. Blatt and V. Weisskopf, **Theoretical Nuclear Physics**, Wiley and Sons, New York (1952) 358.

13. One ϕ in each expression is fixed at zero.

14. The mass scale is adjusted up to the D mass.

15. The three–body branching fractions $B(D \to K\pi\pi)$ are taken from J. Adler *et al.*, SLAC–PUB–4291, submitted to Physical Review Letters. Comparisons between D^0 and D^+ decay modes use the values of σ_{D^0} and σ_{D^+} from this source. The value of $B(D^0 \to \bar{K}^0\pi^+\pi^-)$ is taken from reference 1, and scaled by the new value of σ_{D^0}.

16. The branching fraction to a given final state i is defined as the ratio of the partial width to state i in the absence of other decay modes, divided by the total width. With this definition, the fraction of events in each decay mode that are attributed to the i^{th} component of $\mathcal{L}_{sig}$ is determined by setting f_i equal to its fit value and the other f_j to zero and numerically integrating $\mathcal{L}_{sig}$ across the Dalitz plot, then dividing by the integral of $\mathcal{L}_{sig}$ with all f_j's set to their fit value.

17. M. Aguilar-Benitez *et al.*, Phys. Lett. **170B** (1986) and references therein.

18. The χ^2 measure that we use is defined as $\chi^2 = 2\sum_i n_i \ln(n_i/\mu_i)$, where n_i is the number of events in bin i, μ_i is the number of events predicted by the fit to be in bin i, and the sum is over all bins within the kinematically allowed region of the Dalitz plot. See S. Baker and R. D. Cousins, Nucl. Inst. Meth. **221** (1984) 437.

FIGURE CAPTIONS

1. The Dalitz plot for $D^0 \to K^-\pi^+\pi^0$, and the three projections, shown as data points. The results of the fit are shown as histograms superimposed on the projections. The lower histogram in each projection gives the contribution from background events, while the upper histogram gives the total contribution from signal plus background.
2. The Dalitz plot for $D^0 \to \bar{K}^0\pi^+\pi^-$, and the three projections.
3. The Dalitz plot for $D^+ \to \bar{K}^0\pi^+\pi^0$, and the three projections.
4. The Dalitz plot for $D^+ \to K^-\pi^+\pi^+$, and the three projections.

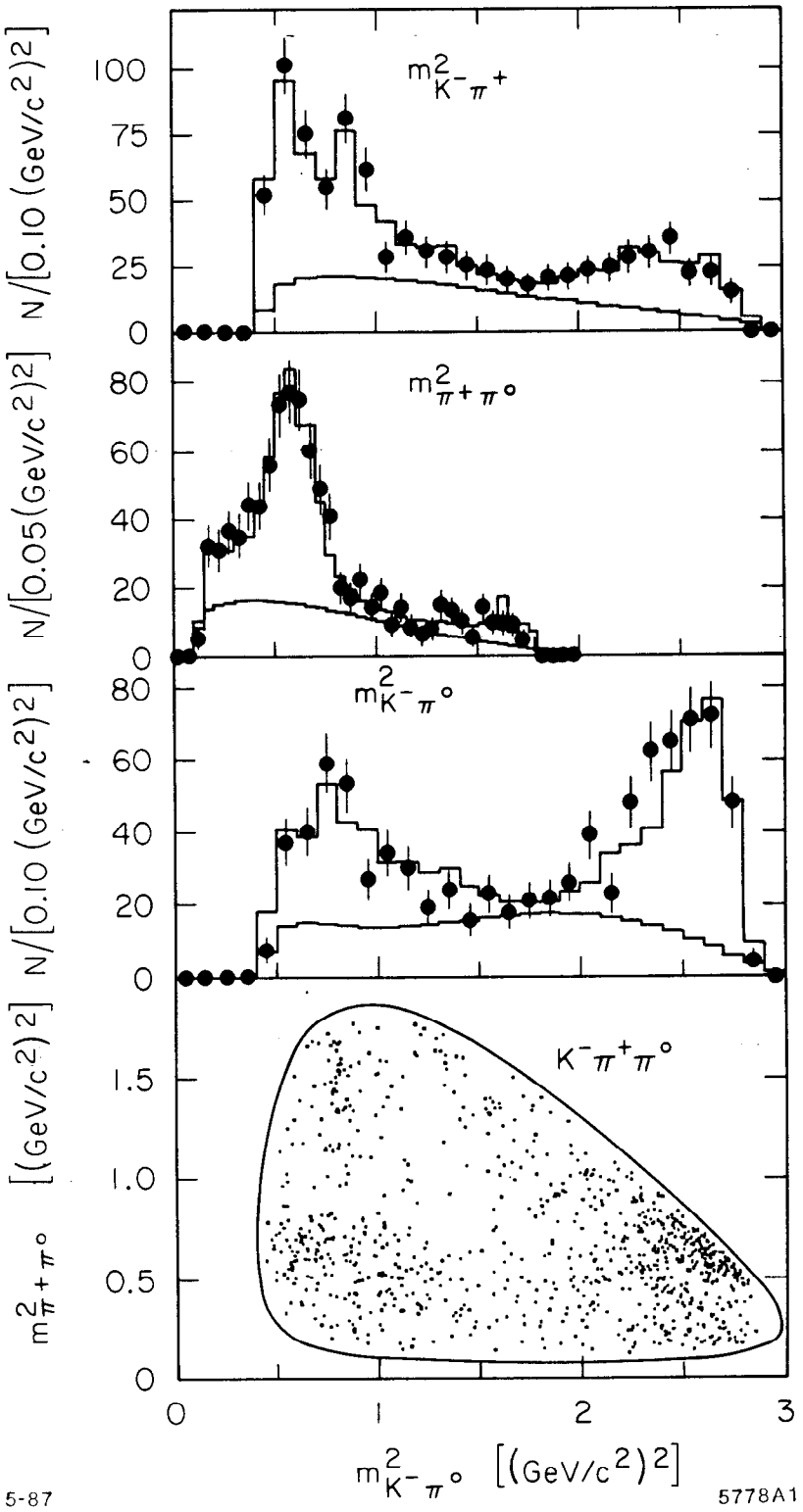
$m^2_{K^-\pi^+}$
$m^2_{\pi^+\pi^\circ}$
$m^2_{K^-\pi^\circ}$
$K^-\pi^+\pi^\circ$
N/[0.10 (GeV/c²)²]
N/[0.05(GeV/c²)²]
N/[0.10 (GeV/c²)²]
$m^2_{\pi^+\pi^\circ}$ [(GeV/c²)²]
$m^2_{K^-\pi^\circ}$ [(GeV/c²)²]
5-87
5778A1

Fig. 1

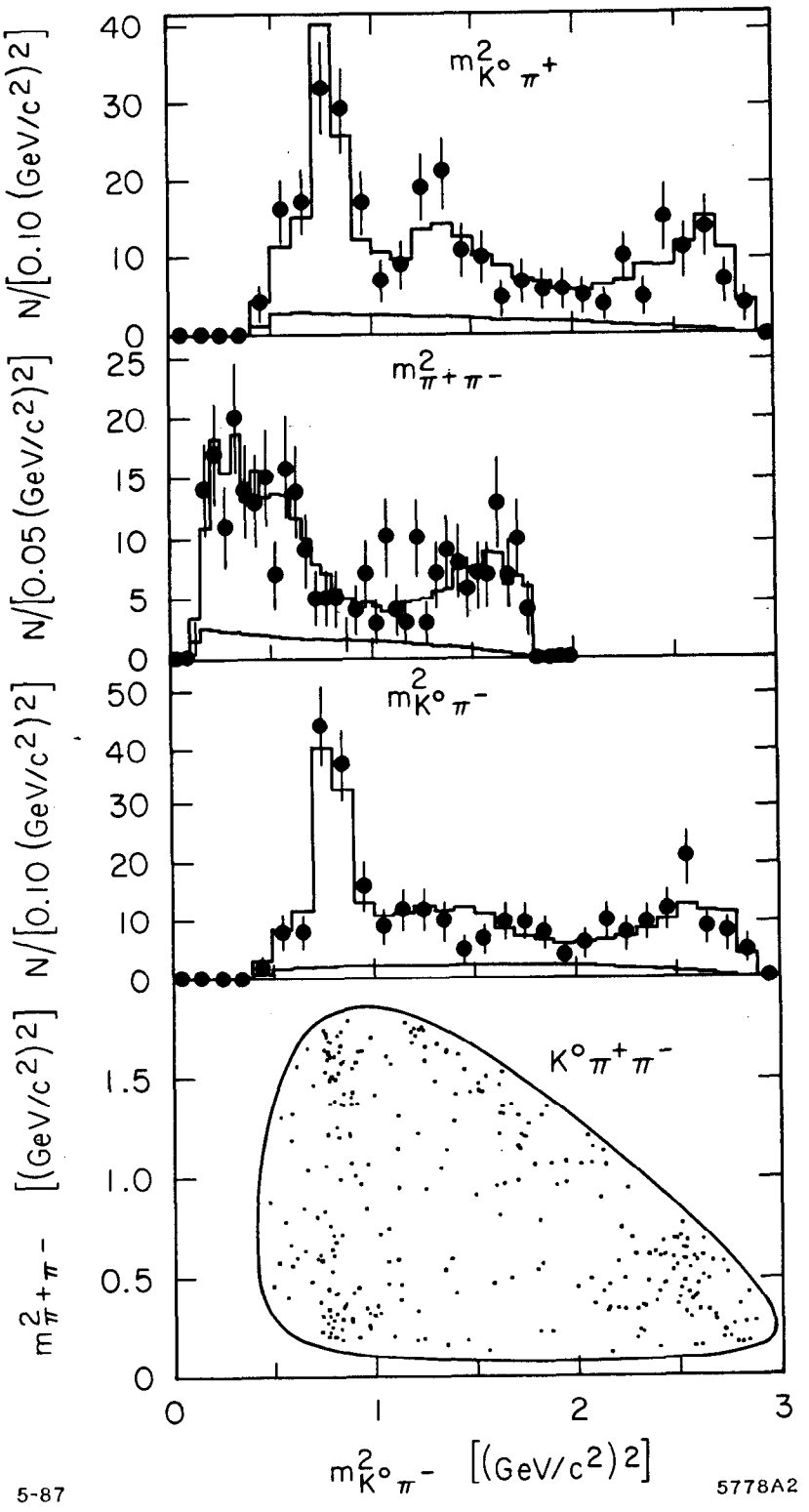
$m^2_{K^0\pi^+}$
$m^2_{\pi^+\pi^-}$
$m^2_{K^0\pi^-}$
$K^0\pi^+\pi^-$
N/[0.10 (GeV/c²)²]
N/[0.05 (GeV/c²)²]
N/[0.10 (GeV/c²)²]
$m^2_{\pi^+\pi^-}$ [(GeV/c²)²]
$m^2_{K^0\pi^-}$ [(GeV/c²)²]
5-87
5778A2

Fig. 2

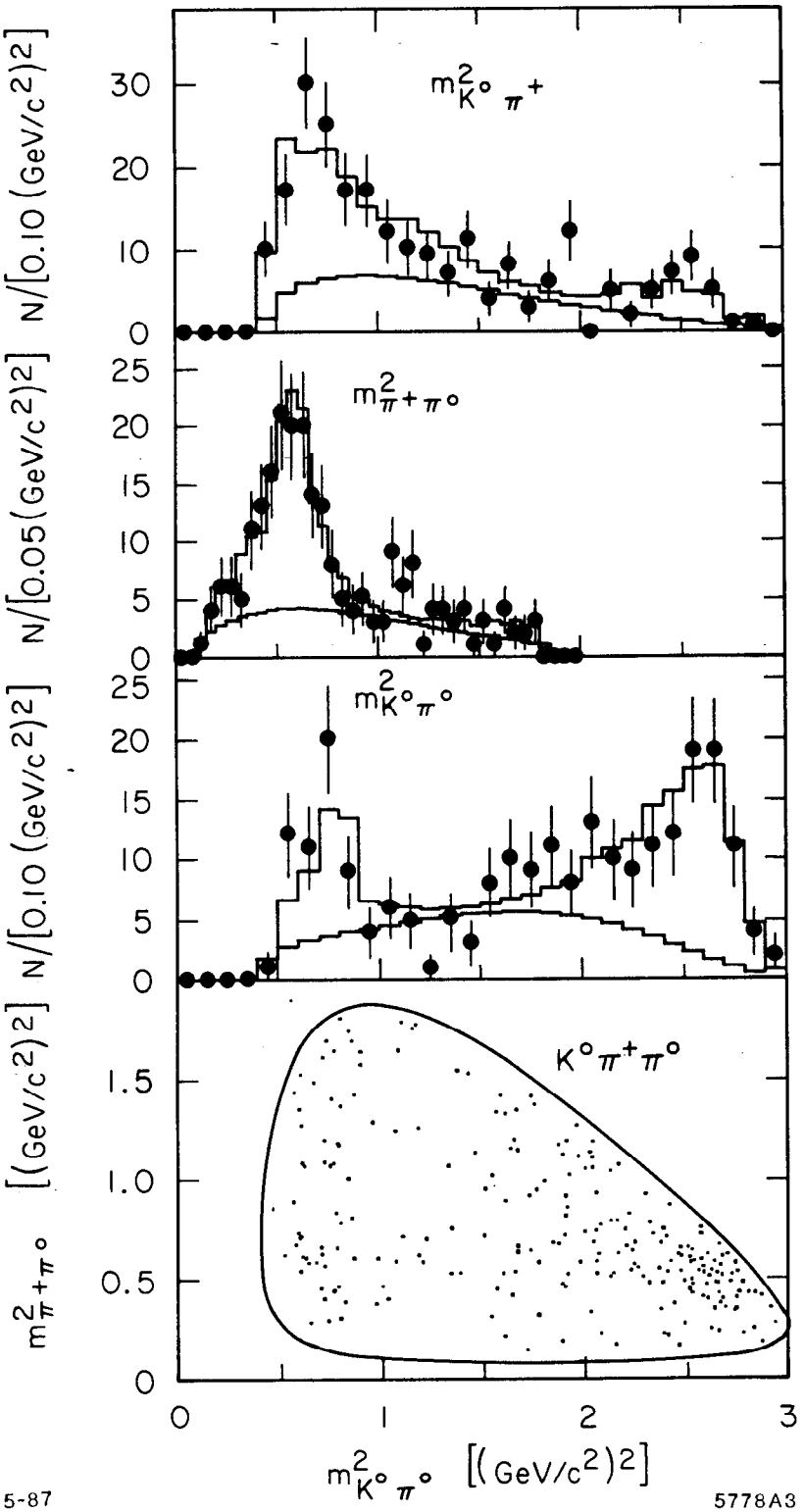
$m^2_{K^0\pi^+}$
$m^2_{\pi^+\pi^0}$
$m^2_{K^0\pi^0}$
$K^0\pi^+\pi^0$
N/[0.10 (GeV/c²)²]
N/[0.05(GeV/c²)²]
N/[0.10 (GeV/c²)²]
$m^2_{\pi^+\pi^0}$ [(GeV/c²)²]
$m^2_{K^0\pi^0}$ [(GeV/c²)²]
5-87
5778A3

Fig. 3

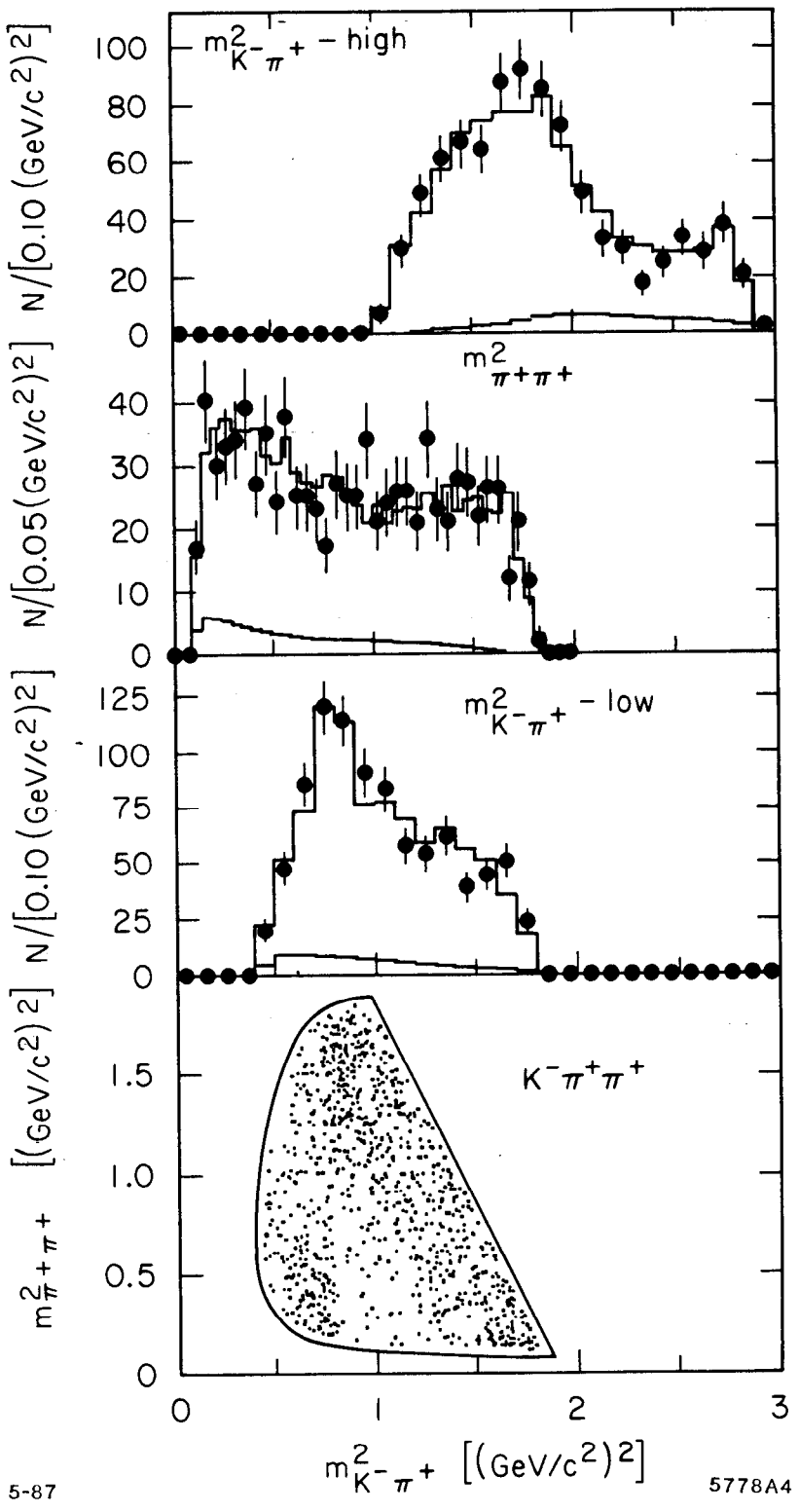
$m^2_{K^-\pi^+}$ – high
$m^2_{\pi^+\pi^+}$
$m^2_{K^-\pi^+}$ – low
$K^-\pi^+\pi^+$
N/[0.10 (GeV/c²)²]
N/[0.05(GeV/c²)²]
N/[0.10 (GeV/c²)²]
$m^2_{\pi^+\pi^+}$ [(GeV/c²)²]
$m^2_{K^-\pi^+}$ [(GeV/c²)²]
5-87
5778A4

Fig. 4